Retrapping Current in Bridge-Type Nano-SQUIDs

D. Hazra, J. R. Kirtley, and K. Hasselbach

Phys. Rev. Applied **4**, 024021 — Published 31 August 2015

DOI: 10.1103/PhysRevApplied.4.024021

Retrapping current in Nano-bridge Superconducting Quantum Interference Devices

D. Hazra[1,2], J.R. Kirtley[1,2,3], and K. Hasselbach[1,2]

[1] *CNRS, Inst NEEL, F-38042 Grenoble, France*

[2] *Univ. Grenoble Alpes, Inst NEEL, F-38000 Grenoble, France and*

[3] *Center for Probing the Nanoscale, Stanford University, Palo Alto, California, U.S.A.*

(Dated: August 10, 2015)

It is a challenge to fabricate nano-bridge Superconducting Quantum Interference Devices (nano-bridge SQUIDs) that operate without hysteresis over a broad temperature range. Hysteresis — defined by the difference between switching- and re-trapping current— is one of the foremost constraints to operating nano-SQUIDs with low noise. The quantum behavior of the switching current has been explored in nano-bridge SQUIDs; but studies exploring parameters ruling the re-trapping current are rare. Here, we study the temperature and magnetic field dependence of the re-trapping current in two different kinds of nano-bridge SQUIDs: tri-layer aluminum-niobium-tungsten nano-bridge SQUIDs and suspended-bridge nano-SQUIDs. Our study confirms previous works showing that the re-trapping current decreases as the bath-temperature increases, and is insensitive to the magnetic field. Using a thermal model originally proposed by Skocpol et al.[1], we account for, and suggest a simple formula which describes, the temperature dependence of the re-trapping current. Our calculations show that the magnitude of the retrapping current is mainly dependent on the superconducting transition temperature and the effective resistance of the weak link, and that the temperature dependence of the retrapping current is ruled by the temperature dependence of the thermal conductivity in the normal and superconducting state. Finally we apply our calculation to newly fabricated shunted nano-bridge SQUIDs, which show non-hysteretic current-voltage characteristics down to at least 250 mK and display systematic voltage modulations as a function of externally applied magnetic fields.

Nano-Superconducting Quantum Interference Devices (Nano-SQUIDs) have been used successfully for many applications, such as to measure the magnetic properties of single nano-particles [2], local magnetic properties with a scanning SQUID microscope [3, 4], and persistent currents of a two dimensional electron gas in a ring [5]. Recent experiments have demonstrated sensitivities which would allow the detection of the magnetic moment of a single electron spin using a Nano-SQUID [6].

Thus, varieties of nano-SQUIDs with different types of junctions— e.g., 3D tunnel junctions [7], 2D bridge type junctions[3, 8–11], superconductor-normal metal-superconductor (SNS) junctions [12], carbon nano-tube junctions[13], 3D bridge type junctions[14] to mention only few— have been developed in the last few decades. That apart, special Nano-SQUIDs, capable of operating at high magnetic field, have been fabricated by various groups [15–17]. Very recently, Schwarz et al., [18] have fabricated $YBa_2Cu_3O_7$ based low-noise nano-SQUIDs, capable of performing magnetization reversal measurements of nano-particles. Out of all these possibilities, because of their relatively simple fabrication process, the nano-bridge SQUIDs remain the most preferred choice of nano-SQUIDs for nano-scale magnetometry.

One of the striking features of such nano-bridge SQUIDs is their hysteretic current-voltage (I-V) characteristic: In a Nano-SQUID, when a current is ramped up from zero, the system remains in the superconducting state until a threshold I_s. At I_s the system switches to a voltage state. After switching, when the current is reduced again, the system regains its superconducting state only at a current I_r which, at low temperatures, is less than I_s.

Hysteresis and the temperature dependence of the I_r have been studied in various Weak-Link (WL) structures such as superconducting Dayem Bridges (DBs) [19], SNS junctions[20], and superconducting nano-wires [21, 22]. To understand the hysteresis phenomena in DBs and nano-wires, Skocpol et al. [1, 21] proposed the following: Upon increasing bias currents from zero, the WL switches to the voltage state at I_s. Once in the voltage state the local temperature T of the WL increases above the bath temperature T_b due to Joule heating. The temperature is highest at the center of the WL and decreases away from the center to eventually reach the bath-temperature. In the voltage state, a self sustained normal region, known as the *hot-spot* and defined by the local temperature $T > T_c$, is created at the center of the WL. The size of the *hot-spot* is a function of the bias-current I and the bath-temperature T_b. When the current is ramped down from above I_s the system regains its superconducting state at a bias current I_r which is smaller than I_s at low temperatures.

The hysteresis is also observed in under-damped tunnel junctions and this is understood by the Resistively and Capacitively Shunted Junction(RCSJ)[23, 24] model. Here, the capacitance across the junction is responsible for the hysteresis[24]. In this model, I_r is proportional to $\sqrt{I_s}$ [23]. The RCSJ model has also been used to explain hysteresis in micro-bridges [25] and SNS [12] junctions. For SNS and Micro-bridges, the capacitance is too small to explain hysteresis using the RCSJ model. Thus, for these cases, the authors introduced the idea of effective capacitance C_{eff}, by equating the RC_{eff} time constant with the relaxation time of the Cooper pairs for micro-bridges [25] and the diffusion time of the Andreev pairs for SNS junctions [12]. Later on, Courtois et. al [20] have shown by directly measuring the electronic temperature that, for SNS junctions the hysteresis is indeed the result of Joule heating. For micro-bridges also, the recent experiments and calculations [19, 21, 22, 26] show that the hysteresis is a result of Joule heating.

In this article we extend the discussion from a single WL to a 2-junction nano-SQUID for two reasons: First, unlike a single WL, in a nano-SQUID, the I_s can be easily modulated using a perpendicular magnetic field, and, therefore, we can readily verify whether I_r is proportional to $\sqrt{I_s}$ or not. Second, understanding and overcoming hysteresis in nano-SQUIDs is essential for their optimal performance [6, 8]. Here, we study the temperature and magnetic field dependence of the I_r in two different types of nano-bridge SQUIDs, tri-layer aluminum-niobium-tungsten nano-bridge SQUIDs and suspended-bridge nano-SQUIDs, down to 250 mK in temperature and 20 mT in magnetic field (limited by our solenoid). We develop a model, using the basic postulates of the *hot-spot* model, to analyze the temperature dependence of I_r. Our work is complementary to previous works in the following ways: In the original paper of Skocpol et al.[1], they ignored the temperature dependence of the thermal conductivity. This leads to a $\sqrt{T_c - T_b}$ [21] temperature dependence of I_r, which doesn't agree with experiment at low temperatures [19, 26]. Tinkham et al.[21] assumed $\kappa_s/\kappa_n = T/T_c$ in a numerical simulation of suspended superconducting nano-wires, where κ_s and κ_n are the thermal conductivities in the normal and superconducting states, respectively, and T_c is the critical temperature. Peng et al. [22] used the exact expression for thermal conductivity (see Eq. 2 below), but they did not take into account the temperature variation of the energy gap; thus in their treatment thermal conductivity shows an unphysical discontinuity , i.e. $f(T) \neq 1$ at $T = T_c$ (see Fig. 4 of [22]). Most recently, Kumar et. al [26] have explored the various thermal regions of a nano-SQUID, but they restricted their studies down to only half of T_c, and they did not theoretically explore I_r. Apart from these hot-spot model based calculations, recently, Vodolazov et al.[27] considered non-equilibrium phenomena responsible for hysteresis in superconducting weak-links. Their theoretical approach, though robust and thorough, is difficult to realize in a real device design. Here, we provide a simple 1-D model which matches well with experiment while taking the temperature dependence of thermal conductivity into account. More importantly, our results involve parameters which can be measured experimentally. Our calculations show that the magnitude of I_r is mainly dependent on the T_c and the effective resistance of the WLs (R_{WL}), and that the temperature dependence of I_r is dependent on the temperature dependence of the thermal conductivity in the normal and superconducting state. We also observe that, unlike I_s, I_r is insensitive to small magnetic fields. Finally we demonstrate the usefulness of our calculation by fabricating shunted nano-bridge SQUIDs that show non-hysteretic current-voltage characteristics at 250 mK and display systematic voltage modulations as a function of externally applied magnetic fields while being biased just above their critical currents.

I. EXPERIMENTS AND RESULTS

We studied two different types of nano-bridge SQUIDs, A and B, with three samples of each type, as listed in Table-I. The A-type devices were tri-layer aluminium-niobium-tungsten(Al-Nb-W) nano-bridge SQUIDs, whereas the B-types were bilayer Al-Nb suspended-bridge Nano-SQUIDs. To see the detailed fabrication methods and schematics for A type nano-bridge SQUIDs see Ref.[28], and for B type see Ref.[29]. Briefly, to fabricate A type nano-bridge SQUIDs, on a bare Si(100) wafer, first W and then Nb films of thickness 80 and 40 nm, respectively, were deposited in situ, using a magnetron-sputtering system. The nano-bridge SQUIDs were patterned using standard Electron Beam Lithography (EBL) and Reactive Ion Etching (RIE) with 20 nm of Al as a etch mask. SF_6 gas was used for RIE of both Nb and W.

To fabricate B-type devices (suspended-bridge nano-SQUIDs), a 30 nm thick Nb film was deposited on a bare Si(100) wafer using electron beam evaporation. Here also the Nano-SQUID patterns were drawn using EBL and RIE. An Al layer of 25 nm thickness was deposited as a mask during RIE. We observed a lateral etching of Nb along with the vertical etching with an approximate ratio of 1:5. Thus, a considerable over-etching of Nb lead to complete removal of Nb under the Al-bridge, producing suspended Al-bridges. For both types of nano-bridge SQUIDs the patterns were designed to allow a four terminal resistance measurement.

In Fig. 1a, we present a schematic top view of our devices, defining the length ($2L$) and width (w) of nano-bridges. Fig. 1b and 1c show different layers near the nano-bridges for type-A (tri-layer Al-Nb-W) and type-B (suspended-bridge) nano-bridge SQUIDs, respectively.

Fig. 2 shows the DC I-V characteristics at 400 mK for sample A1 (tri-layer Al-Nb-W nano-bridge SQUID) at different magnetic fields (from 0 to 20 mT). We see that I_s modulates between $I_{s,min}$ and $I_{s,max}$, whereas I_r does not have any detectable magnetic field dependence. The dotted arrows show the time evolution of the voltage, confirming hysteresis. The T_c of the nano-bridge SQUIDs, listed in Table-I, is defined at the minimum bath temperature where I_c is zero, i.e, the DC I-V characteristic is linear. The inset of the Fig. 2 shows a Scanning Electron Micrograph (SEM) image of A1. The reported sample has a size of 2.5 μm (i.e., a loop area of 6.25 μm^2). The other geometrical parameters are listed in Table-I.

Fig. 3 plots the temperature dependence of the I_r for B-type (suspended-bridge) nano-bridge SQUIDs, whereas the inset shows the same for A-type (tri-layer Al-Nb-W) nano-bridge SQUIDs. The magnitudes of I_r for A-type nano-bridge SQUIDs varies due to differences in the widths of the weak link. For both types of nano-bridge SQUIDs, I_r saturates for temperatures below approximately half of the T_c.

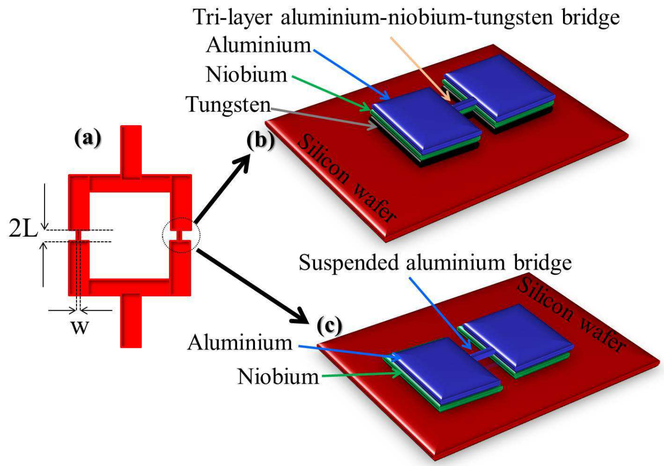

FIG. 1. (a) The schematic top view of a typical nano-bridge SQUID. (b) and (c) show the various layers for type-A (tri-layer Al-Nb-W nano-bridge SQUID) and -B (suspended-bridge) devices, respectively. The dimensions are not to scale.

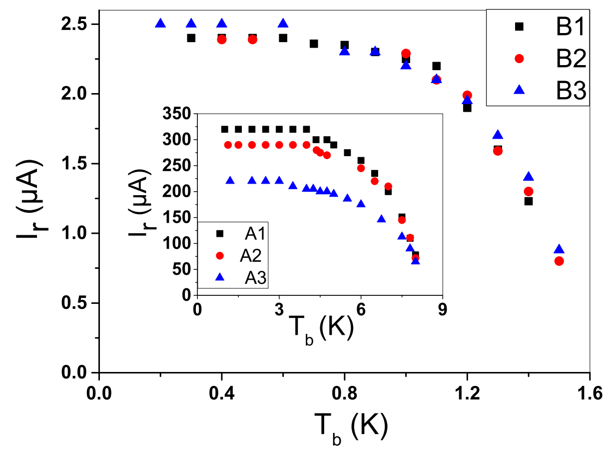

FIG. 3. The temperature dependence of the re-trapping current for B1 (square), B2 (dot), and B3 (triangle). The inset shows the same for A1(square) A2(dot), and A3. I_r has little temperature dependence below $T_c/2$.

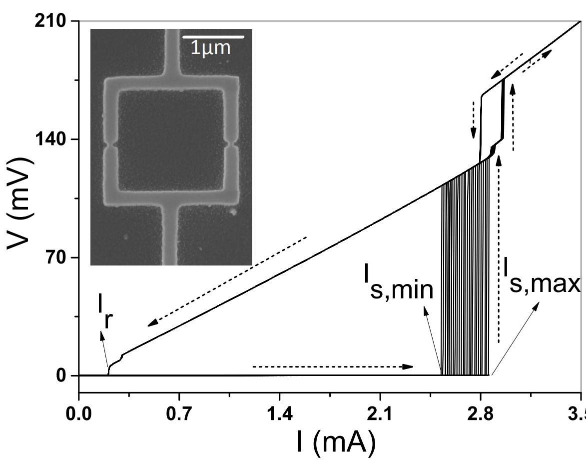

FIG. 2. (a) The DC I-V characteristic at 1 K for A1, (tri-layer Al-Nb-W nano-bridge SQUID) at different magnetic fields. The switching current I_s is modulated between $I_{s,max}$ and $I_{s,min}$, whereas I_r is insensitive to magnetic field. The dotted arrows show the direction of current sweeps, evidencing voltage hysteresis. The insets show the SEM image of A1.

II. A MODEL CALCULATION

In this section, we develop a model for the temperature dependence of I_r of nano-bridge SQUIDs based on the hypothesis of Skocpol et al. [1, 21]. Before exploring the exact nano-SQUID geometry, let us first consider, for simplicity, a superconducting WL, connecting two large superconducting pads, as shown in Fig. 1. Later, we shall extend our calculation to the nano-SQUID geometry. The temperature profile of a WL in the voltage state has been described in many articles [1, 19, 21]. Here, we focus on the dependence of I_r on the bath temperature.

In the voltage state, because of the Joule-heating, the local temperature (T) of the bridge increases above the bath temperature T_b. We assume that the connecting pads, being massive, act as a thermal bath to ensure the thermalization of the two ends of the WL to T_b. In general, for a sufficiently large bias-current, the local temperature at the connecting pads can be increased above T_b [1, 19]; but here we focus on I_r. We also assume that the temperature at the center ($x = 0$) of the bridge is higher than T_c, i.e., is in the normal state. At $x = \pm\, x_0$, away from the center, the local temperature decreases to T_c, defining normal metal-superconductor (N-S) interfaces. Thus, this model assumes the existence of a self-sustained normal region (hot-spot) of length $2x_0$. We also assume a quasi-equilibrium state, so that we can define a local temperature T.

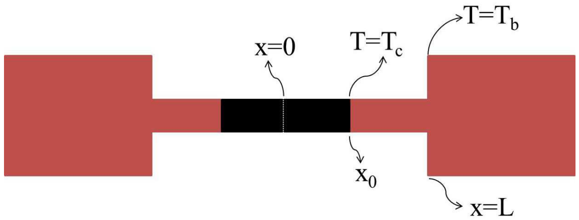

FIG. 4. The schematic diagram of a current-biased superconducting-bridge of length $2L$, connecting two bulk electrodes. The black portion at the center represents the *hot-spot* in the voltage state. $x = \pm x_0$, where $T = T_c$, define N-S interfaces. The contact pads at $x = \pm L$ thermalize the edges of the bridge to the bath temperature.

We shall now focus on the heat flow mechanism in the normal-state near I_r. The generated Joule-heat can be removed either by thermal conduction or surface heat loss across the bridge-substrate interface. As has been shown earlier [19, 22], thermal conduction is much more efficient than surface heat loss for this kind of geometry. In our calculation we ignore the surface-heat loss altogether. We subsequently show that a simple linear-model of the thermal conductivity is sufficient to explain the T_b dependence of I_r . We also derive an analytical expression for I_r, showing good agreement with the experiments.

The heat flow equation in the voltage state for the superconducting section ($x_0 \leq x < L$) of the bridge can be written as:

$$-\kappa_s A \frac{dT}{dx} = I^2 R(x_0) \qquad (x_0 \leq x < L). \tag{1}$$

Here, κ_s is the electronic part of the thermal conductivity in the superconducting state, R is the resistance of the normal section and A is the cross-sectional area of the bridge. Since the experiments were performed at very low temperatures, we can ignore the phonon contribution to the thermal conductivity. The temperature dependence of κ_s can be expressed using the following formula [30]:

$$f(T) = \kappa_s/\kappa_n = \frac{3}{2\pi^2}\int_{\frac{\Delta(T)}{\kappa_B T}}^{\infty} \left(\frac{x}{\cosh(x/2)}\right)^2 dx. \tag{2}$$

Here, κ_n is the electronic part of the thermal conductivity in the normal state and $\Delta(T)$ is the superconducting energy gap at temperature T. κ_n can be calculated using the Wiedemann-Franz law: $\kappa_n = L_0 T/\rho_n$, where L_0 is the Lorentz number and ρ_n is the normal state resistivity of the material. This expression allows us to express κ_s in terms of ρ_n which is more easily accessible experimentally.

For a given I, the resistance can be written as $R(x_0) = R_{WL}(x_0/L)$, where R_{WL} is the normal state resistance of the entire WL.

Eq. 1 can now be re-written as:

$$tf(t)\frac{dt}{dx} = -\frac{I^2}{I_0^2}\frac{1}{L}\frac{x_0}{L} \qquad (x_0 \leq x < L). \tag{3}$$

Here, $t = T/T_c$ is the normalized temperature, and $I_0 = \sqrt{2L_0}\ T_c/R_{WL}$ is the natural current-scale of the problem. In re-writing Eq. 1 we have expressed κ_s in terms of ρ_n and also made use of the relation: $R_{WL} = 2\rho_N\ L/\ A$.

At a fixed $t_b = T_b/T_c$, to calculate x_0 as a function of bias-current I we impose the boundary conditions $t = t_b$ at $x = L$, and $t = 1$ at $x = x_0$. This leads to

$$\int_{t_b}^{1} tf(t)\,dt = -\frac{I^2}{I_0^2}\frac{1}{L}\frac{x_0}{L}\int_{L}^{x_0} dx = -\frac{I^2}{I_0^2}\frac{1}{L}\frac{x_0}{L}(L - x_0) \tag{4}$$

Thus, re-arranging Eq. 4, I as a function of x_0 becomes

$$I^2 = I_0^2 \frac{L^2}{x_0(L - x_0)} g(t_b), \tag{5}$$

where we have defined

$$g(t_b) = \int_{t_b}^{1} tf(t)\,dt. \tag{6}$$

Now we recollect that I_r is the minimum current required to maintain an N-S interface. Minimizing I with respect to x_0, from Eq. 5, we get the following expression for I_r:

TABLE I. Experimental and fit parameters for all the samples. Here d is the thickness of various layers, w and ℓ are the width and length of the WLs, and T_c (exp) is the experimental critical temperature. 1, 2, and 3 stand for fit parameters for (1) $f(t)$ (Eq.2), (2) $f(t) = t$, and (3) $f(t) = t^2$.

Sam. no.	d_W (nm)	d_{Nb} (nm)	d_{Al} (nm)	w (nm)	$2L$ (nm)	T_c (exp) (K)	R_{WL} (1) (Ω)	R_{WL} (2) (Ω)	R_{WL} (3) (Ω)
A1	80	40	30	90	100	8.25± 0.10	10.5	9.9	8.5
A2	80	40	30	80	100	8.25± 0.10	8.0	7.5	6.5
A3	80	40	30	60	100	8.25± 0.10	7.2	6.8	5.9
B1	-	30	25	40	200	1.60± 0.05	175.5	165.5	142.7
B2	-	30	25	40	200	1.60± 0.05	176.2	166.2	143.3
B3	-	30	25	40	200	1.60± 0.05	168.5	158.9	137.0

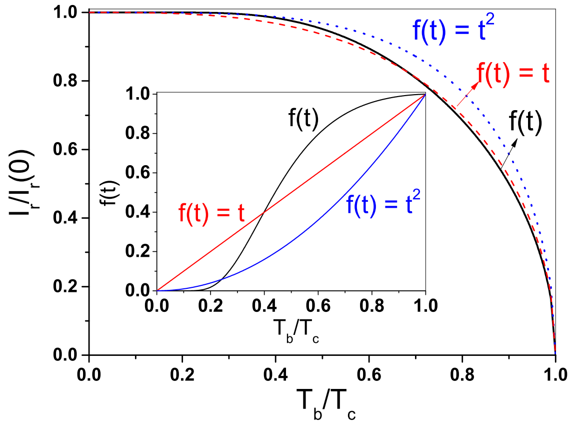

FIG. 5. The theoretical predictions showing the variation of the normalized I_r as a function of normalized T_b for $f(t)$ (Eq.2), $f(t) = t$, and $f(t) = t^2$; the corresponding $I_r(0)$ is $1.23I_0$, $1.15I_0$, and I_0, respectively. The inset shows the variation of $f(t)$ (Eq.2), $f(t) = t$, and $f(t) = t^2$.

$$I_r(t_b) = 2\frac{\sqrt{2L_0}T_c}{R_{WL}}\sqrt{g(t_b)}. \quad (7)$$

The t_b dependence of I_r, as Eq. 7 suggests, depends, via Eq. 2 and Eq. 6, on the temperature dependence of the thermal conductivity $f(t)$. Before we solve numerically, in order to have a better physical insight, let us try to find an approximate analytical expression for $f(t)$. Since at $T = 0$, κ_s should be zero (i.e. $f(t) = 0$), and at $T = T_c$ (i.e. at $t = 1$), κ_s should be equal to κ_n (i.e. $f(t) = 1$), we take the following approximation: $f_t = t^n$, where n is a constant. In this case, Eq. 7 becomes

$$I_r(t_b) = \sqrt{\frac{4}{n+2}}\frac{\sqrt{2L_0}T_c}{R_{WL}}\sqrt{1 - t_b^{n+2}}. \quad (8)$$

In Fig. 5, we plot the variation of I_r as a function of T_b in normalized units for the exact expression of $f(t)$ following Eq. 2, and also for $f(t) = t$ (i.e. for $n = 1$) and $f(t) = t^2$ (i.e. for $n = 2$). The inset shows the temperature dependence of $f(t)$ following Eq. 2, and also for $f(t) = t$ and $f(t) = t^2$. To evaluate $f(t)$ numerically we have made use of the approximation to the full BCS expression $\Delta/\Delta(0) = \sqrt{(1-t)}$, with $\Delta(0)\ /\ \kappa_B\ T_c = 1.76$ [23]. From Fig. 6, we see that $f(t) = t$ is closer to the actual expression (Eq. 2) in predicting the temperature variation of I_r than $f(t) = t^2$. This is because I_r involves the integral of $f(t)$, and as the inset of Fig. 6 suggests, for half of the temperature range t is smaller than $f(t)$ (Eq. 2) while for the remaining half it is bigger, and thus in the integration process they compensate each other. On the other hand, t^2 is almost always smaller than $f(t)$ (Eq. 2), underestimating I_r.

To extend this model from a single WL to a nano-bridge SQUID (two parallel WLs, connected in a superconducting ring), we note that, at a fixed t_b, the product of I_r and R_{WL} is constant (Eq. 7). From an analogy with a parallel resistor network, this implies that if two WLs are connected in parallel, the net I_r would be the sum of two individual WLs' I_r. Thus, the above calculations can be extended — without any loss of generality — to nano-SQUID structures. In particular, as soon as in one of the two junctions the hot spot disappears, that is when I_{bias} becomes lower than I_r (retrapping current), the Joule self heating disappears, the current passes without dissipation through this junction. The current sustaining the self heating of the other branch is immediately diverted to the superconducting branch ($I_c > 2 \times I_r$) . In the absence of Joule heating the latter hotspot disappears and the second nano bridge becomes superconducting, and thus the entire SQUID. Such dynamic processes on short time scales are beyond the time window of our measurements, but may deserve further investigation.

III. ANALYSIS AND DISCUSSIONS

In this section we first compare the experimental data with our theoretical calculations. In Fig. 6, we plot a universal curve of I_r, for all six samples (dots), in normalized units. The experimental I_r has been normalized with respect to the value measured at the lowest temperature. The lines show the fits for $f(t)$ (Eq. 2), $f(t) = t$, and $f(t) = t^2$. For clarity, $f(t) = t$ and $f(t) = t^2$ have been shifted

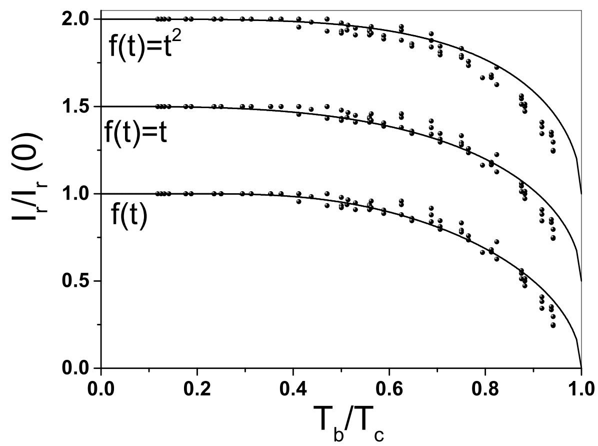

FIG. 6. Universal curve (dots) of I_r, normalized with respect to the value measured at the lowest temperature, for all six samples. The lines show the theoretical predictions for (from bottom) $f(t)$ (Eq.2), $f(t) = t$, and $f(t) = t^2$. The fitting parameter $R_W L$ is listed in Table-I for all three cases. For clarity, $f(t) = t$ and $f(t) = t^2$ have been shifted vertically by 0.5 and 1, respectively.

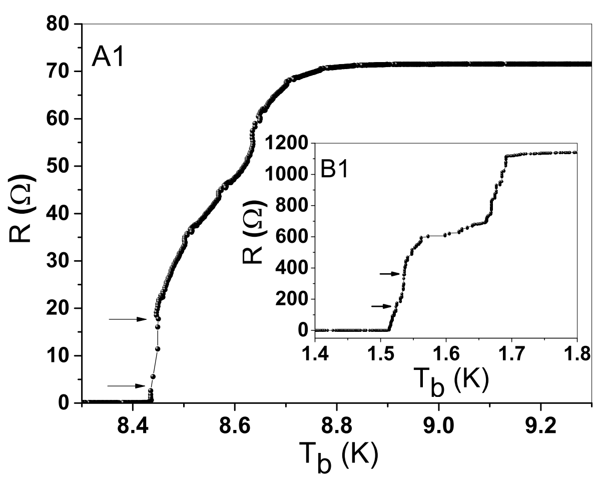

FIG. 7. The temperature variation of the resistance for A1 (tri-layer Al-Nb-W nano-bridge SQUID) near T_c. The inset shows the same for B1(suspended bridge nano-SQUID). The measurement was done using a lock-in at frequency 1117 Hz and a bias current of 1 μA for A1 and 100 nA for B1. The broad transition reflects the onset of the superconductivity at different temperatures for different sections of the devices. The two arrows show the last two transitions, possibly reflecting the onset of the superconductivity in the nano-bridges.

vertically by 0.5 and 1, respectively. The fit parameter R_{WL} is listed in Table-I for all three cases. The standard deviations are 0.04, 0.05, and 0.07 for $f(t)$, $f(t) = t$, and $f(t) = t^2$, respectively. As expected, the best-fit is observed for the exact expression of $f(t)$ (Eq. 2). Between the two approximate expressions, $f(t) = t$ provides the better fit, as expected.

Next we extract R_{WL} from the experimental curves, and compare with theoretical fits. In general, the resistance — measured from the slope of the I-V curve in the linear regime, i.e., at high bias current — is a few times higher than R_{WL}. This is because at high bias-current the N-S interface may occur well inside the electrode. Near I_r, the I-V characteristic is highly non-linear, making it difficult to measure R_{WL} from the slope. Thus, to estimate R_{WL}, we perform direct resistance measurements as a function of temperature with a small bias-current. Since the widths of the different parts of our nano-bridge SQUIDs vary considerably — the bridges are $\sim$ 50 nm, the nano-SQUID arms are $\sim$ 350 nm, and the bonding pads are $\sim$ 250 μm — the T_c of the different parts would also differ considerably; the bonding pads should have the highest T_c, whereas the WLs should have the lowest T_c. In Fig. 7, we plot the temperature variation of the resistance for A1 (tri-layer Al-Nb-W nano-bridge SQUID). The inset shows the temperature variation of the resistance for B1(suspended bridge nano-SQUID). The measurement was performed using a lock-in at frequency 1117 Hz and bias currents of rms amplitude 1 μA and 100 nA were applied for A1 and B1, respectively. The onset of T_c for different regions of the device occur at different temperatures, as expected. The broadening of the final resistance tail makes it difficult to estimate R_{WL}. We thus try to trace the last two transitions, shown by the arrows, to estimate R_{WL}. From this, we estimate R_{WL} for A1 between 18 and 5 Ω and for B1 between 350 and 150 Ω. Apart from observing the resistance transition, we also estimate R_{WL} from normal resistance and the known geometry of our nano-bridge SQUIDs. For A1, the normal resistance, as we see from Fig. 7, is $\sim 71.0\ \Omega$, which is the total contribution from bonding pads, narrow-leads, SQUID arms, and WLs. These, as we know from SEM images and our EBL drawing, corresponds to $30R_\square$ altogether, where $R_\square$ is the square resistance of the films. From this we estimate $R_{WL} \sim 2.6\ \Omega$ for A1. This is less than the value from either the fit or from the R-T curve. Thus, the effective lengths of the WLs are actually longer than their geometrical lengths, implying that the hot-spot extends beyond the WL into the electrode even at very small currents. We can still use Eq. 7, but with R_{WL} replaced by an effective WL resistance $R_{WL,eff}$. For suspended-bridge nano-SQUIDs, the absence of a Nb layer in the bridge makes it difficult to estimate R_{WL} from geometry.

Next we compare the re-trapping currents for the two kinds of SQUIDs. From Fig. 3, we see that type-A devices (tri-layer Al-Nb-W nano-bridge SQUIDs) have much higher I_rs than type-B devices (suspended-bridge nano-SQUIDs). In type-A devices, the superconducting properties are dictated by Nb, whereas Al and W provide thermalization to the bridge, and also help reduce the effective R_{WL}. For type-B devices, the T_c is dictated by aluminum, which has a lower T_c than Nb. The higher T_c and lower effective R_{WL} results in higher I_r for type-A devices in comparison to type-B, as expected from Eq. 7. In addition, since part of the bridge is normal just above I_r, a fraction of the current may pass through the Al and W layers for type-A devices, further enhancing their re-trapping currents.

Finally we apply our model to design and fabricate non-hysteretic nano-bridge SQUIDs, which can be read-out continuously. Hysteresis can be suppressed either by increasing I_r, decreasing I_s, or both simultaneously. As we learned from our discussion, I_r can be increased by reducing the effective R_{WL}. This has been achieved by fabricating a bi-layer Al-Nb nano-bridge SQUID on a continuous W film, as shown in Fig. 8. The fabrication process is similar to an A-type (tri-layer Al-Nb-W) nano-bridge SQUID, except that only the Nb layer has been etched. The underneath W layer has been left unaffected, which reduces the effective R_{WL} by thermalizing the WLs and shunting a fraction of the bias current. The thickness of the Al, Nb, and W films are respectively 20, 25, and 80 nm, whereas the lengths and widths of the bridges are ~ 180 and 40 nm, respectively. The presence of the normal layer of W reduces T_c ($2.0\ K$) by proximity effect.

Fig. 9a shows the DC I-V characteristic at 250 mK, confirming a significant reduction in hysteresis; although we still see a sharp jump near the transition. The inset shows the AC I-V characteristic, measured using a lock-in at frequency 1117 HZ, demonstrating the absence of the sharp jump near the transition. This is because the nano-SQUID remains in the superconducting state for part of the applied sinusoidal signal (see Fig. 3 of Ref. 28). From the DC I-V characteristic, we get $I_r \sim 20\ \mu$A. This, from Eq. 7, gives an effective $R_{WL} \sim 27\ \Omega$ for $T_c = 2K$. On the other hand, the WL resistance estimated from the normal resistance of a tri-layer Al-Nb-W film of the same width and length (see Fig. 1 of [28]) is $\sim 18\ \Omega$, comparable to the effective R_{WL}. Thus the presence of a W film underneath restricts the N-S interface very close to the WL. It also reduces the switching current I_s by proximity effect, further reducing the hysteresis.

Next we demonstrate the performance of our devices. Fig. 9b shows the voltage modulation of the nano-bridge SQUID as a function of an externally applied magnetic field at different rms current amplitudes. Here also the experiment was performed using a lock-in at 1117 Hz frequency. The systematic voltage modulation clearly demonstrate that the nano-bridge SQUID can be read out continuously down to at least 250 mK. To estimate the flux-noise Φ_n, we bias the device at the most sensitive point of the flux-voltage (Φ-V) characteristic (maxima of $\frac{\partial V}{\partial \Phi} = V_\Phi$) and measure the voltage noise V_n. The Φ_n was then estimated from the formula [31] $\Phi_n = V_n/V_\Phi$. The voltage noise spectra shows that we are limited by our

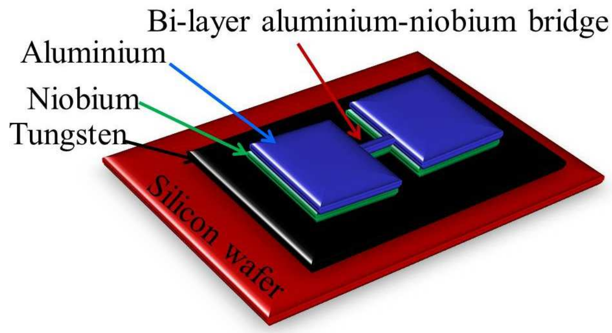

FIG. 8. The schematic view near the nano-bridge of the shunted non-hysteretic bi-layer nano-SQUID of Al-Nb. The SQUID was patterned on a W film which reduces the normal resistance and also acts as an efficient heat sink.

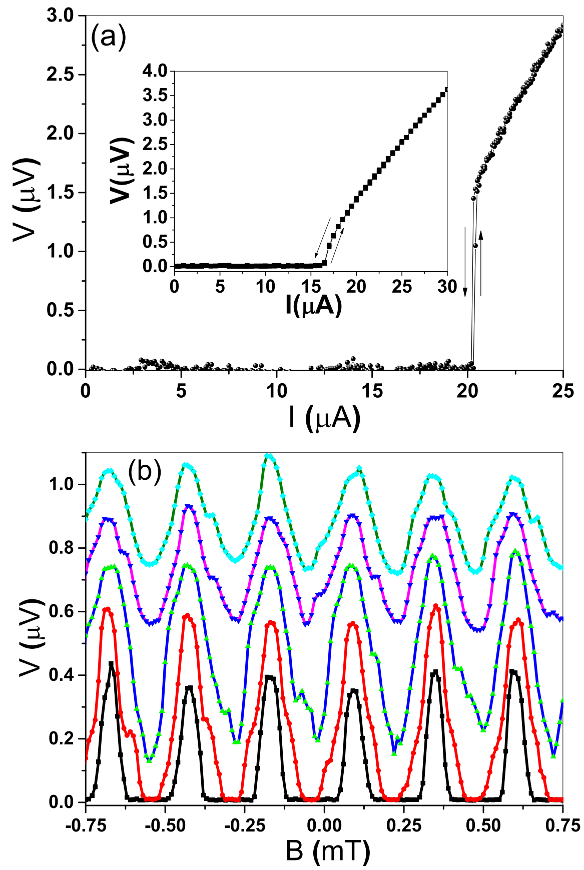

FIG. 9. (a) The DC I-V characteristic of the shunted nano-bridge SQUID at 250 mK showing the reduction of hysteresis. The inset shows the AC I-V characteristic (rms values) of the same device measured at 1117 Hz using a lock-in. (b) The voltage modulation of the nano-bridge SQUID as a function of magnetic fields at different bias currents: 16.0, 16.5, 17.0, 17.5, and 18.0 μA from the bottom.

room temperature amplifier noise ~ 1 nV/$\sqrt{Hz}$. For our sample, $V_\Phi \sim 2.5$ μV/ Φ_0 which translates to a spectral density of flux noise, assuming a voltage noise density of the room temperature amplifiers of 1 nV/$\sqrt{Hz}$, to 4.5 $\times$ 10^{-4} $\Phi_0/\sqrt{Hz}$. This result is encouraging for further development of Nb/W devices, as ours were operated in an unshielded environment and room temperature electronics were used. We expect that low temperature amplification schemes will lead to a significant reduction in the voltage noise. The ability of the nano-bridge SQUID to operate in a continuous manner at such a low temperature makes it a useful tool to study the ground state properties of quantum systems.

In summary, we studied the temperature and magnetic field dependence of the re-trapping current in two different kinds of devices: tri-layer aluminum-niobium-tungsten nano-bridge SQUIDs and suspended-bridge nano-SQUIDs. The re-trapping current was seen to be insensitive to the magnetic field, but decreased as the bath-temperature increased. Using a thermal model, we accounted for the temperature dependence of the re-trapping current. We also suggested a simple analytical expression to fit the temperature dependence of the re-trapping current. Our theory showed good agreement with experiment. Our calculations showed that the magnitude of I_r was mainly dependent on the T_c and the effective resistance of the WLs (R_{WL}), and that the temperature dependence of I_r was dependent on the temperature dependence of the thermal conductivity in the normal and superconducting state. We applied our theory to successfully fabricate non-hysteretic nano-bridge SQUIDs capable of performing continuous read-out down to at least 250 mK, which can be useful to study the ground state of quantum systems.

Acknowledgements: D. Hazra and J.R. Kirtley acknowledge support from the Grenoble Nanosciences Fondation within the project "Chair of Excellence Super-

NanoCharac". J.R. Kirtley was also supported by the NSF under Grant No. PHY-0425897. The authors thank T. Crozes for e-beam lithography training and E. André for thin film preparation.

---

[1] W. J. Skocpol, M. R. Beasley, and M. Tinkham, Self-heating hotspots in superconducting thin-film microbridges, J. Appl. Phys. **45**, 4054 (1974).

[2] W. Wernsdorfer, Classical and quantum magnetization reversal studied in nanometer-sized particles and clusters, Adv. Chem. Phys. **118**, 99 (2001).

[3] K. Hasselbach, C. Veauvy, D. Mailly, MicroSQUID magnetometry and magnetic imaging, Physica C **332**, 140 (2000).

[4] L. Embon, Y. Anahory, A. Suhov, D. Halbertal, J. Cuppens , A. Yakovenko, A.Uri, Y. Myasoedov, M. L. Rappaport, M. E. Huber, A. Gurevich, and E.Zeldov, Probing dynamics and pinning of single vortices in superconductors at nanometer scales, Scientific Reports, **5**, 7598. (2015).

[5] D. Mailly, C. Chapelier, and A. Benoit, Experimental observation of persistent currents in GaAs-AlGaAs single loop, Phys. Rev. Lett. **70**, 2020 (1993).

[6] D. Vasyukov, Y. Anahory, L. Embon, D. Halbertal, J. Cuppens, L. Neeman, A. Finkler, Y. Segev, Y. Myasoedov, M. L. Rappaport, M. E. Huber, and E. Zeldov, A scanning superconducting quantum interference device with single electron spin sensitivity, Nature Nanotechnology **8**, 639 (2013).

[7] C. Granata, A. Vettoliere, R. Russo, M. Fretto, N. De Leo, and V. Lacquaniti, Three-dimensional spin nanosensor based on reliable tunnel Josephson nano-junctions for nanomagnetism investigations, Appl. Phys. Lett. **103**, 102602 (2013).

[8] L. Hao, J. C. Macfarlane, J. C. Gallop, D. Cox, J. Beyer, D. Drung, and T. Schurig, Measurement and noise performance of nano-superconducting-quantum-interference devices fabricated by focused ion beam, Appl. Phys. Lett. **92**, 192507 (2008).

[9] S. K. H. Lam and D. L. Tilbrook, Development of a niobium nanosuperconducting quantum interference device for the detection of small spin populations, Appl. Phys. Lett. **82**, 1078 (2003).

[10] A. G. P. Troeman, H. Derking, B. Borger, J. Pleikies, d. Veldhuis, and H. Hilgenkamp, NanoSQUIDs Based on Niobium Constrictions, Nano Lett. **7**, 2152 (2007).

[11] K. Hasselbach, D. Mailly, and J. R. Kirtley, Micro-superconducting quantum interference device characteristics, J. Appl. Phys. **91**, 4432 (2002).

[12] L. Angers, F. Chiodi, G. Montambaux, M. Ferrier, S. Guéron, H. Bouchiat, and J. C. Cuevas, Proximity dc squids in the long-junction limit, Phys. Rev. B **77**, 165408 (2008).

[13] J. P. Cleuziou, W. Wernsdorfer, V. Bouchiat, T. Ondarcuhu, and M. Monthioux, Carbon nanotube superconducting quantum interference device, Nature Nanotech., **1** 53 (2006).

[14] R. Vijay, E. M. Levenson-Falk, D. H. Slichter, and I. Siddiqi, Approaching ideal weak link behavior with three dimensional aluminum nanobridges, **96**, 223112 (2010).

[15] L. Chen, W. Wernsdorfer, C. Lampropoulos, G. Christou, and I. Chiorescu,On-chip SQUID measurements in the presence of high magnetic fields, Nanotechnology **21**, 405504 (2010).

[16] S. Mandal, T. Bautze, O. A. Williams, C. Naud, È. Bustarret, F. Omnès, P. Rodière, T. Meunier, C. Bäuerle, and L. Saminadayar, The Diamond Superconducting Quantum Interference Device, ACS Nano **5**, 7144 (2011).

[17] R. Wolbing, J. Nagel, T. Schwarz, O. Kieler, T. Weimann, J. Kohlmann, A. B. Zorin, M. Kemmler, R. Kleiner, and D. Koelle, Nb nano superconducting quantum interference devices with high spin sensitivity for operation in magnetic fields up to 0.5 T, Appl. Phys. Lett. **102**, 192601 (2013).

[18] T. Schwarz , R. Wölbing, C. F. Reiche, B. Müller, M. J. Martínez-Pérez, T. Mühl, B. Büchner, R. Kleiner and D. Koelle, Low-Noise $YBa_2Cu_3O_7$ Nano-SQUIDs for Performing Magnetization-Reversal Measurements on Magnetic Nanoparticles, Phys. Rev. Applied, **3**, 044011 (2015).

[19] D. Hazra, L. M. A. Pascal, H. Courtois, and A. K. Gupta,

Hysteresis in superconducting short weak links and μ-SQUIDs, Phys. Rev. B **82**, 184530 (2010).

[20] H. Courtois, M. Meschke, J. T. Peltonen, and J. P. Pekola, Origin of Hysteresis in a Proximity Josephson Junction, Phys. Rev. Lett. **101**, 067002 (2008).

[21] M. Tinkham, J. U. Free, C. N. Lau, and N. Markovic, Hysteretic IV curves of superconducting nanowires, Phys. Rev. B **68**, 134515 (2003).

[22] Peng Li, Phillip M. Wu, Yuriy Bomze, Ivan V. Borzenets, Gleb Finkelstein, and A. M. Chang, Retrapping current, self-heating, and hysteretic current-voltage characteristics in ultranarrow superconducting aluminum nanowires, Phys. Rev. B **84**, 184508 (2011).

[23] M. Tinkham, Introduction to Superconductivity 2nd ed. (Mc Graw-Hill, New York, 1996).

[24] W. C. Stewart, Current–voltage characteristics of Josephson junctions, Appl. Phys. Lett.**12**, 277 (1968); D. E. McCumber, Effect of ac Impedance on dc Voltage–Current Characteristics of Superconductor WeakLink Junctions, J. Appl. Phys.**39**, 3113 (1968).

[25] Y. Song, Origin of capacitance in superconducting microbridges, J. Appl. Phys. **47**, 2651 (1976).

[26] Nikhil Kumar, T. Fournier, H. Courtois, C. B. Winkelmann, and Anjan K. Gupta, Reversibility Of Superconducting Nb Weak Links Driven By The Proximity Effect In A Quantum Interference Device, Phys. Rev. Lett. **114**, 157003 (2015).

[27] D. Yu. Vodolazov and F. M. Peeters, Origin of the hysteresis of the current voltage characteristics of superconducting microbridges near the critical temperature, Phys. Rev. B **84**, 094511 (2011).

[28] D. Hazra, J.R. Kirtley, and K. Hasselbach, Nano-superconducting quantum interference devices with continuous read out at milliKelvin temperatures, Appl. Phys. Lett. **103**, 093109 (2013).

[29] D. Hazra, J.R. Kirtley, and K. Hasselbach, Nano-superconducting quantum interference devices with suspended junctions, Appl. Phys. Lett **104**, 152603 (2014).

[30] A. A. Abrikosov, Fundamentals of the Theory of Metals, (Elsevier Science, Amsterdam, 1988).

[31] J. Clarke and A. I. Braginski, The SQUID Handbook, Vol-1, (WILEY-VCH Verlag GmbH and Co. KGaA, 2004).